Gating effects in antiferromagnetic CuMnAs

M. J. Grzybowski (iD) , P. Wadley, K. W. Edmonds, R. P. Campion, K. Dybko (iD) , M. Majewicz, B. L. Gallagher, M. Sawicki (iD) , and T. Dietl (iD)

View Online   Export Citation   CrossMark

ARTICLES YOU MAY BE INTERESTED IN

Spin current detection in antiferromagnetic CuMnAs
Applied Physics Letters **115**, 182407 (2019); https://doi.org/10.1063/1.5121739

Magnetic properties of bismuth substituted yttrium iron garnet film with perpendicular magnetic anisotropy
AIP Advances **9**, 115001 (2019); https://doi.org/10.1063/1.5122998

Investigation of magnetism and magnetic structure of anti-ThCr$_2$Si$_2$-type Tb$_2$O$_2$Bi by magnetization and neutron diffraction measurements
AIP Advances **9**, 115301 (2019); https://doi.org/10.1063/1.5126399

Gating effects in antiferromagnetic CuMnAs

View Online   Export Citation   CrossMark

M. J. Grzybowski,[1,2,a)] (ID) P. Wadley,[3] K. W. Edmonds,[3] R. P. Campion,[3] K. Dybko,[1,2] (ID) M. Majewicz,[2]
B. L. Gallagher,[3] M. Sawicki,[2] (ID) and T. Dietl[1,4,b)] (ID)

AFFILIATIONS

[1] International Research Centre MagTop, Institute of Physics, Polish Academy of Sciences, Aleja Lotnikow 32/46, PL-02668 Warsaw, Poland
[2] Institute of Physics, Polish Academy of Sciences, Aleja Lotnikow 32/46, PL-02668 Warsaw, Poland
[3] School of Physics and Astronomy, University of Nottingham, Nottingham NG7 2RD, United Kingdom
[4] WPI-Advanced Institute for Materials Research, Tohoku University, Sendai 980-8577, Japan

[a)] Electronic mail: grzybowski@MagTop.ifpan.edu.pl. **Currently at:** Eindhoven University of Technology, 5600 MB Eindhoven, The Netherlands.
[b)] Electronic mail: dietl@MagTop.ifpan.edu.pl

ABSTRACT

Antiferromagnets (AFs) attract much attention due to their potential applications in spintronics. Both the electric current and the electric field are considered as tools suitable to control the properties and the Néel vector direction of AFs. Among AFs, CuMnAs has been shown to exhibit specific properties that result in the existence of the current-induced spin-orbit torques commensurate with spin directions and topological Dirac quasiparticles. Here, we report on the observation of a reversible effect of an electric field on the resistivity of CuMnAs thin films, employing an ionic liquid as a gate insulator. The data allow us to determine the carrier type, concentration, and mobility independent of the Hall effect that may be affected by an anomalous component.

The interest in antiferromagnetic (AF) spintronics is stimulated by an increasing number of reports on different scenarios of manipulation of the Néel vector. Current-driven methods include spin-orbit torque commensurate with spin directions[1–6] or antidamping torque.[7–9] Although they provide means to reversibly control the Néel vector direction, they require a high current density. On the other hand, switching by an electric *field* is considered promising for low-power spintronics. The electric field has been shown to modify the magnetic behavior of numerous ferromagnetic (FM) materials,[10–15] surprisingly also including rather conductive metal films,[15–17] presumably because of an important role played by interfacial magnetic anisotropy.[18] It was also shown that an electric field can decrease the switching current in FM tunneling junctions.[19] As for AFs, the electric field was proven to change the domain structure of multiferroic BiFeO$_3$[20] or switch between AF and FM interactions in EuTiO$_3$.[21] The magnetoelectric effect was also utilized to construct a memory device in the α-Cr$_2$O$_3$ film.[22] Metallic AFs were observed to exhibit the modulation of the exchange spring effect[23,24] or to change the magnetoresistance in AF-FM heterostructures[25]

due to the electric field. Finally, it has been recently demonstrated that it is possible to influence the spin-orbit torque by applying an electric field to a piezoelectric substrate.[26] Furthermore, theoretical studies of CuMnAs show the coexistence of massless Dirac fermions and the AF order.[27,28] The reorientation of the Néel vector can induce the topological metal-insulator transition.[27,28] However, to observe these phenomena experimentally, tuning the Fermi level to the bandgap with an electric field would be highly desirable. In this context, exploring the influence of an electric field on CuMnAs is important from the point of view of low-power spintronics, topological aspects of AFs, and fundamental research on the role of electric fields in AFs.

In this paper, we demonstrate experimentally that the resistivity of highly conducting antiferromagnetic tetragonal CuMnAs thin films passivated by AlO$_x$ is reversibly modulated at room temperature by an electric field applied across an ionic liquid. The sign and the magnitude of the effect allow us to evaluate the carrier type, concentration, and mobility. By comparing the field and Hall effect data, we assess a possible magnitude of the anomalous

Hall resistance. Conversely, under an assumption that the anomalous Hall resistance is negligible in collinear AFs, the consistency of the field and Hall effect results demonstrates that phenomena associated with surface charge trapping states,[29] electromigration,[30] and piezoelectricity[31] are weak in CuMnAs so that the main effect of gating is the formation of depletion and accumulation layers for positive and negative gate voltages, respectively. The study also yields an upper limit for the dependence of the resistivity modulation on the direction of the current with respect to crystal axes.

The field and Hall effect data have been obtained for a 10 nm CuMnAs tetragonal film grown coherently on a (001) GaAs substrate by molecular beam epitaxy and capped with a 2.5 nm Al layer that undergoes oxidation in the air. The thickness of the capping layer corresponds to the thickness of native Al oxide.[32] Additionally, Hall measurements have been carried out for a 45 nm film of CuMnAs grown on a (001) GaP substrate and also capped with a 2.5 nm Al layer for data validation. Two devices have been prepared from the 10 nm film. The first one (device A) has been obtained from an elongated piece of the epilayer by fixing gold wires with silver paint and by depositing a droplet of the ionic liquid DEME-TFSI between them. As shown schematically in Fig. 1, about a half of the sample is covered by the gate. Another gold wire is dipped in the ionic liquid so that it does not touch the studied layer and forms a gate electrode. Microdevice B has been fabricated by means of multilevel electron beam lithography, wet etching, and lift-off to pattern four different current paths and eight gold contact pads, and by employing atomic layer deposition for growing an Al_2O_3 film serving to protect the etched trenches from undesired oxidation or chemical reaction with ionic liquid, as shown in Fig. 2. A wire bonder is used to fix wire probes to the contact pads. Similar to device A, the ionic liquid drop, deposited on the device top, and the gate electrode wire complete the field-effect structure. In the case of microdevice B, the gate area is much larger than the central probed region.

The capacitance per unit area $C/S = (4.4 \pm 0.8) \times 10^{-7}$ F/cm^2 has been estimated for our ionic liquid by the $C–V$ profiling, employing the frequency of 1 kHz and the modulation voltage of 30 mV superimposed on the dc voltage between 0 and 1 V. This means that we can change interfacial charge density by about 3×10^{12} cm^{-2} by the gate voltage of $V_G = 1$ V.
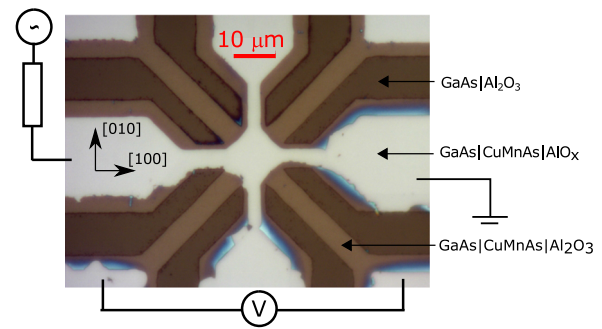
FIG. 2. Microdevice (device B) with eight contacts (clear bluish areas) for studies of the field effect for current along different crystalline axes. The darkest regions are trenches etched down to the substrate defining current paths, covered additionally by an Al_2O_3 film (brown areas) with atomic layer deposition to prevent chemical reactions between the layer and the ionic liquid. The Al_2O_3 film extends beyond the etched trenches covering partially the CuMnAs layer to ensure there is no contact with side walls and the ionic liquid. The whole device is covered by the ionic liquid in which the gate electrode is dipped. The current and voltage connections are shown for resistance measurements along the [100] crystal direction.

The Hall resistance measured for our films is linear in the magnetic field in the studied range up to 9 T and reveals a positive sign of the Hall coefficient, in agreement with earlier studies.[33] Since magnetization of collinear AFs and, thus, spin polarization of band carriers vary also linearly with the magnetic field, the Hall resistance may *a priori* contain an anomalous component. Neglecting it, and adopting a single band transport model, our measurements lead to the values of hole concentrations p and mobilities μ_H, collected in Table I. The value $p = 1.1 \times 10^{22}$ cm^{-3} determined previously[33] lies between $p = (1.50 \pm 0.02) \times 10^{22}$ and $(0.5 \pm 0.1) \times 10^{22}$ cm^{-3} obtained here for the 45 and 10 nm thick films, respectively. A relatively small hole density in the thinnest layer, corresponding to the areal density of 5×10^{15} cm^{-2}, may point to interfacial or surface depletion. At the same time, the magnitudes of the Hall mobilities are within 3.6 ± 0.3 cm^2/V s for the three films in question. A comparison of these values to the field mobilities will tell about the role of surface states as well as to what extent the Hall data are affected by multiband transport and the anomalous Hall effect in the semimetallic and antiferromagnetic CuMnAs.

The key experiment of this work is the field effect, i.e., how the four-probe longitudinal resistance changes under the influence of the gate voltage. The main challenge is a high value of the carrier concentration in CuMnAs, making the magnitude of the field effect small and comparable to resistance changes caused by temperature fluctuations under ambient conditions. Therefore, a strong electric field has to be used and a good temperature stabilization has to be implemented. Accordingly, the studied devices are mounted on a sample holder in a vacuum chamber of a cryostat with a temperature controller, the arrangement preventing also a contact with water vapor in the air. The gate voltage is applied to the gate electrode in the form of a square wave with a period of 200 or 300 s. In the case of device A, the current source supplies a probing current I in the range 1–100 μA of alternating polarity (20 s period) to eliminate thermal forces. In the case of device B, resistance changes generated by the gate voltage are probed by an ac lock-in method with an excitation
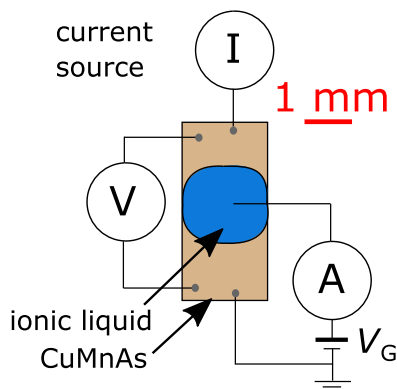

FIG. 1. Experimental setup for the determination of the resistivity changes under the influence of the gate voltage (V_G) for device A. The blue circle denotes the area covered with the ionic liquid.

TABLE I. Properties of two CuMnAs films at room temperature determined from Hall measurements: the Hall coefficient R_H, hole concentration p, and mobility μ_H evaluated by neglecting a possible contribution from the anomalous Hall effect.

CuMnAs layer thickness (nm)	T (K)	$R_H \times 10^8$ (Ω cm/T)	$p \times 10^{-21}$ (cm^{-3})	μ_H (cm^2/V s)
45	300	4.1 ± 0.1	15.0 ± 0.2	3.9 ± 0.1
10	283	13 ± 4	5 ± 1	3.4 ± 0.7

current of 10 μA and frequency 11 Hz. The device design allows us to probe resistance along four different crystal axes, [100], [110], [010], and [1$\bar{1}$0].

As shown in Figs. 3 and 4, clear variations of the resistance with the same periodicity as the gate voltage are observed for both devices. Assuming that neither electrochemical nor piezoelectric effects operate, an increase in resistance for positive values of the gate voltage means that hole carriers are involved. The field-effect data are presented in the form of relative resistance changes $\Delta R_{xx}/R_{xx}$,

$$\frac{\Delta R_{xx}}{R_{xx}} = \frac{R_{xx}(V_G) - R_{xx}(V_G = 0\,\text{V})}{R_{xx}(V_G = 0\,\text{V})}, \quad (1)$$

which is as a difference between the resistance when a specific gate voltage is on and when the gate voltage is zero, normalized by the resistance value at $V_G = 0$. In the case of device A, a small resistance drift linear in time is observed and subtracted from the data. It originates probably from a chemical reaction between the ionic liquid and edges of the sample. Its rate is 9×10^{-5} Ω/s for $V_G = 1$ V, but for most gate voltages used in the experiment it does not exceed 6×10^{-5} Ω/s. The signal measured in the case of device B (Fig. 4)

exhibits larger noise compared to device A (Fig. 3), which is likely caused by the small potential variations due to the chemical processes occurring away from the central device region where the ionic liquid spreads.

The resistance changes depend on the magnitude of the gate voltage (Fig. 5), whereas they do not show any clear dependence on the probing current (Fig. 6). The current flowing through the gate I_G (Fig. 3) decays with time. This dependence is presumably a long-time tail of two phenomena: (i) the capacitance charging effect via a nonzero resistance of the sample and (ii) a reorganization process of the charge distribution within the ionic liquid.[34,35] For the smaller device B, the total current through the gate does not exceed 10 nA, which means that its magnitude in the probed region is much below 1 nA. V_G has been used in the range between −1 V and 1 V. A significant increase in I_G and R_{xx} for V_G beyond this range suggests the onset of chemical reactions and electrical breakdown.

A linear fit to the experimental data for device A presented in Fig. 5 indicates that the relative resistivity change $\Delta R_{xx}/R_{xx} = (3.1 \pm 0.5) \times 10^{-4}$ per 1 V in the studied gate voltage range. The corresponding values for device B are also shown for measurements carried out for different current directions with respect to crystal axes, and a linear fit to these data gives $\Delta R_{xx}/R_{xx} = (5 \pm 1) \times 10^{-4}$ per 1 V. Within the estimated experimental uncertainty, there is no dependence of $\Delta R_{xx}/R_{xx}$ on the current direction. The lower value
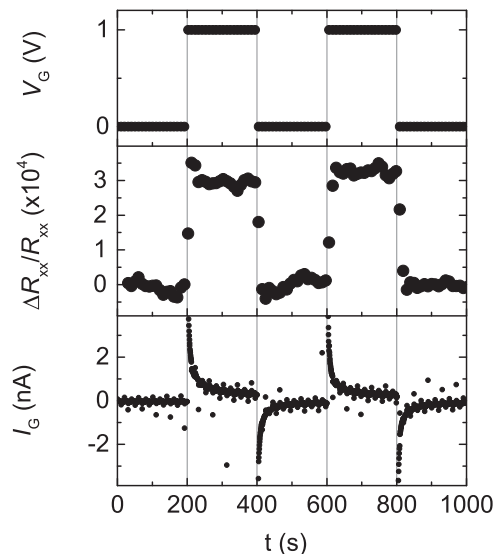
FIG. 3. Time dependence of the gate voltage V_G, relative resistance changes $\Delta R_{xx}/R_{xx}$, and current flowing through the gate I_G for device A at room temperature for 10 μA probing current in the experimental setup presented in Fig. 1. A clear correlation between changes in the gate voltage and longitudinal resistance can be seen, whereas the residual gate current I_G shows a different time dependence.
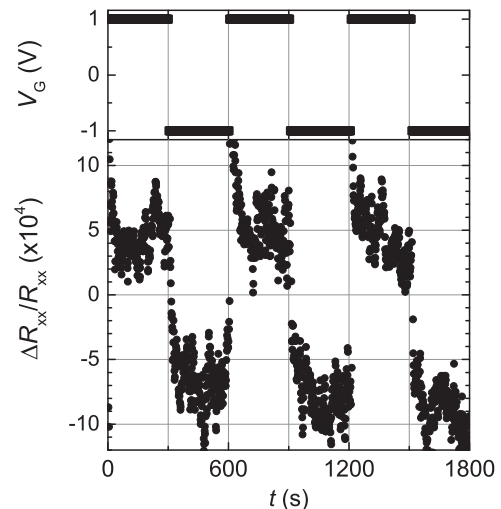
FIG. 4. Relative resistance changes $\Delta R_{xx}/R_{xx}$ for device B under the influence of the gate voltage V_G of the magnitude shown in the upper panel. The current is flowing along the [100] crystal direction.
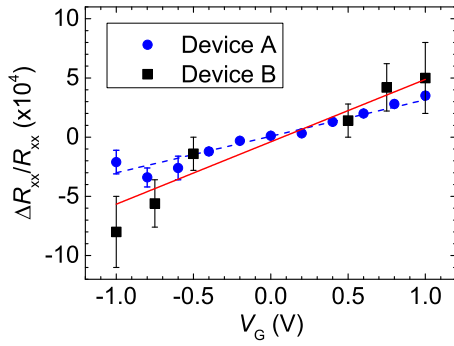
FIG. 5. Dependence of the relative resistance changes $\Delta R_{xx}/R_{xx}$ on the gate voltage V_G for the two studied structures. The lines represent a linear fit to the experimental data for the device A (dashed, blue line) and device B (solid, red line).

of $\Delta R_{xx}/R_{xx}$ in the case of device A is assigned to only partial covering of the region between the voltage probes by the ionic liquid, as shown in Fig. 1. Actually, the data for these two samples are in accord if corrected by a factor f describing a relative coverage of the probed area by the ionic liquid, where $f = 0.5 \pm 0.1$ and $f = 1$ for devices A and B, as shown in Figs. 1 and 2, respectively.

We compare the experimental values of $\Delta R_{xx}/R_{xx}$ to theoretical estimations under the assumption that the only effect of the gate electric field is a depletion or accumulation of hole carriers at the layer surface. Under this assumption, a change in the areal hole density Δp in the gated region is given by

$$\Delta p = -\frac{CV_G}{Sq}, \qquad (2)$$

where $C/S = (4.4 \pm 0.8) \times 10^{-7}$ F/cm^2 and $q = e$ for holes. On the other hand, assuming that the hole mobility μ is independent of the local carrier density as well as noting that in our case $\Delta p \ll pt$, where t is the film thickness,

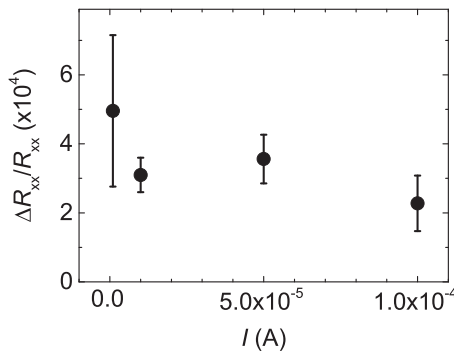$$\frac{\Delta R_{xx}}{R_{xx}} = -f \frac{\Delta p}{pt}. \qquad (3)$$

FIG. 6. Relative resistance changes $\Delta R_{xx}/R_{xx}$ in device A recorded for different values of probing currents I at $V_G = 1$ V. No apparent dependence is found in the studied current range, as expected.

TABLE II. Comparison of the Hall (μ_H) and field mobility (μ_E) for studied devices.

	μ_H (cm^2/V s)	μ_E (cm^2/V s)
Device A	. . .	3.7 ± 1
Device B	3.4 ± 0.7	3.7 ± 1

For the areal hole concentration determined from the Hall measurements $(5 \pm 1) \times 10^{15}$ cm^{-2}, we arrive to $\Delta R_{xx}/R_{xx} = f \cdot (5 \pm 1) \times 10^{-4}$ per 1 V, which is in good agreement with the experimentally observed values presented in Fig. 5 for both devices taking into account the values of f quoted above.

The Hall effect and the resistivity changes generated by gating allow us to compare the values of carrier mobility, namely, the Hall mobility, $\mu_H = \sigma_{xx}/pq$, and the field mobility, μ_E, defined by

$$\mu_E = -\frac{1}{C/S} \frac{\partial \sigma_\square}{\partial V_G}, \qquad (4)$$

where $\sigma_\square$ is the sheet conductivity in the gated region. In terms of the device longitudinal resistance R_{xx}, μ_E assumes the form

$$\mu_E = \frac{L}{fWC/S} \frac{1}{R_{xx}^2} \frac{\partial R_{xx}}{\partial V_G}, \qquad (5)$$

where L and W is the length and the width of the probed region, respectively; $L/W = 1.7 \pm 0.3$ and 1 ± 0.1 for devices A and B, respectively. The mobility values determined from the data in Fig. 5 and Eq. (5) for the studied structure are presented in Table II. The numbers quoted there imply that hole concentrations determined from the Hall resistance on the one hand and from the field mobility and sample conductance on the other hand are in accord.

In summary, the electric field can modify reversibly the resistivity of the CuMnAs structure capped with AlO$_x$. A quantitative agreement between the values of the Hall and field mobilities proves that the modulation of the itinerant hole concentration in the surface layer is a mechanism accounting for the observed field effect. This points out that within the studied range of the electric fields, electrochemical and piezoelectric phenomena as well as charging of surface states do not contribute significantly to the field-induced resistance changes, at least at room temperature. At the same time, there is no indication for a sizable contribution of the anomalous Hall effect. Similarly, there is no evidence for a breakdown of the single band approximation, as in the case of the multiband transport the Hall effect would provide information of the highest mobility carriers, whereas the field effect on the band with the largest density of states at the Fermi energy. The presented approach opens a way to manipulate the Fermi level and to explore the influence of the electric field on the magnetic order and the Néel vector switching in conducting antiferromagnetic systems.

REFERENCES

[1] J. Železný, H. Gao, K. Výborný, J. Zemen, J. Mašek, A. Manchon, J. Wunderlich, J. Sinova, and T. Jungwirth, "Relativistic Néel-order fields induced by electrical current in antiferromagnets," Phys. Rev. Lett. **113**, 157201 (2014).

[2] P. Wadley, B. Howells, J. Zelezny, C. Andrews, V. Hills, R. P. Campion, V. Novak, K. Olejnik, F. Maccherozzi, S. S. Dhesi, S. Y. Martin, T. Wagner, J. Wunderlich, F. Freimuth, Y. Mokrousov, J. Kunes, J. S. Chauhan, M. J. Grzybowski, A. W. Rushforth, K. W. Edmonds, B. L. Gallagher, and T. Jungwirth, "Electrical switching of an antiferromagnet," Science **351**, 587–590 (2016).

[3] M. J. Grzybowski, P. Wadley, K. W. Edmonds, R. Beardsley, V. Hills, R. P. Campion, B. L. Gallagher, J. S. Chauhan, V. Novak, T. Jungwirth, F. Maccherozzi, and S. S. Dhesi, "Imaging current-induced switching of antiferromagnetic domains in CuMnAs," Phys. Rev. Lett. **118**, 057701 (2017).

[4] P. Wadley, S. Reimers, M. J. Grzybowski, C. Andrews, M. Wang, J. S. Chauhan, B. L. Gallagher, R. P. Campion, K. W. Edmonds, S. S. Dhesi, F. Maccherozzi, V. Novak, J. Wunderlich, and T. Jungwirth, "Current polarity-dependent manipulation of antiferromagnetic domains," Nat. Nanotechnol. **13**, 362–365 (2018).

[5] M. Meinert, D. Graulich, and T. Matalla-Wagner, "Electrical switching of antiferromagnetic Mn₂Au and the role of thermal activation," Phys. Rev. Appl. **9**, 064040 (2018).

[6] S. Y. Bodnar, L. Šmejkal, I. Turek, T. Jungwirth, O. Gomonay, J. Sinova, A. A. Sapozhnik, H. J. Elmers, M. Kläui, and M. Jourdan, "Writing and reading antiferromagnetic Mn₂Au by Néel spin-orbit torques and large anisotropic magnetoresistance," Nat. Commun. **9**, 1–7 (2018).

[7] X. Z. Chen, R. Zarzuela, J. Zhang, C. Song, X. F. Zhou, G. Y. Shi, F. Li, H. A. Zhou, W. J. Jiang, F. Pan, and Y. Tserkovnyak, "Antidamping-torque-induced switching in biaxial antiferromagnetic insulators," Phys. Rev. Lett. **120**, 207204 (2018).

[8] T. Moriyama, K. Oda, T. Ohkochi, M. Kimata, and T. Ono, "Spin torque control of antiferromagnetic moments in NiO," Sci. Rep. **8**, 14167 (2018).

[9] L. Baldrati, O. Gomonay, A. Ross, M. Filianina, R. Lebrun, R. Ramos, C. Leveille, F. Fuhrmann, T. R. Forrest, F. Maccherozzi, S. Valencia, F. Kronast, E. Saitoh, J. Sinova, and M. Kläui, "Mechanism of Néel order switching in antiferromagnetic thin films revealed by magnetotransport and direct imaging," Phys. Rev. Lett. **123**, 177201 (2019).

[10] H. Ohno, D. Chiba, F. Matsukura, T. Omiya, E. Abe, T. Dietl, Y. Ohno, and K. Ohtani, "Electric-field control of ferromagnetism," Nature **408**, 944–946 (2000).

[11] H. Boukari, P. Kossacki, M. Bertolini, D. Ferrand, J. Cibert, S. Tatarenko, A. Wasiela, J. A. Gaj, and T. Dietl, "Light and electric field control of ferromagnetism in magnetic quantum structures," Phys. Rev. Lett. **88**, 207204 (2002).

[12] D. Chiba, M. Sawicki, Y. Nishitani, Y. Nakatani, F. Matsukura, and H. Ohno, "Magnetization vector manipulation by electric fields," Nature **455**, 515–518 (2008).

[13] M. Sawicki, D. Chiba, A. Korbecka, Y. Nishitani, J. A. Majewski, F. Matsukura, T. Dietl, and H. Ohno, "Experimental probing of the interplay between ferromagnetism and localization in (Ga, Mn)As," Nat. Phys. **6**, 22–25 (2010).

[14] D. Chiba, S. Fukami, K. Shimamura, N. Ishiwata, K. Kobayashi, and T. Ono, "Electrical control of the ferromagnetic phase transition in cobalt at room temperature," Nat. Mater. **10**, 853–856 (2011).

[15] F. Matsukura, Y. Tokura, and H. Ohno, "Control of magnetism by electric fields," Nat. Nanotechol. **10**, 209–220 (2015).

[16] M. Weisheit, S. Fahler, A. Marty, Y. Souche, C. Poinsignon, and D. Givord, "Electric field-induced modification of magnetism in thin-film ferromagnets," Science **315**, 349–351 (2007).

[17] P. Maruyama, Y. Shiota, T. Nozaki, K. Ohta, N. Toda, M. Mizuguchi, A. A. Tulapurkar, T. Shinjo, M. Shiraishi, S. Mizukami, Y. Ando, and Y. Suzuki, "Large voltage-induced magnetic anisotropy change in a few atomic layers of iron," Nat. Nanotechnol. **4**, 158–161 (2009).

[18] T. Nozaki, A. Kozioł-Rachwał, M. Tsujikawa, Y. Shiota, X. Xu, T. Ohkubo, T. Tsukahara, S. Miwa, M. Suzuki, S. Tamaru, H. Kubota, A. Fukushima, K. Hono, M. Shirai, Y. Suzuki, and S. Yuasa, "Highly efficient voltage

[19] control of spin and enhanced interfacial perpendicular magnetic anisotropy in iridium-doped Fe/MgO magnetic tunnel junctions," NPG Asia Mater. **9**, e451 (2017).

[19] W.-G. Wang, M. Li, S. Hageman, and C. L. Chien, "Electric-field-assisted switching in magnetic tunnel junctions," Nat. Mater. **11**, 64–68 (2012).

[20] T. Zhao, A. Scholl, F. Zavaliche, K. Lee, M. Barry, A. Doran, M. P. Cruz, Y. H. Chu, C. Ederer, N. Spaldin, R. R. Das, D. M. Kim, S. H. Baek, C. B. Eom, and R. Ramesh, "Electrical control of antiferromagnetic domains in multiferroic BiFeO₃ films at room temperature," Nat. Mater. **5**, 823–829 (2006).

[21] P. J. Ryan, J.-W. Kim, T. Birol, P. Thompson, J.-H. Lee, X. Ke, P. S. Normile, E. Karapetrova, P. Schiffer, S. D. Brown, C. J. Fennie, and D. G. Schlom, "Reversible control of magnetic interactions by electric field in a single-phase material," Nat. Commun. **4**, 1334 (2013).

[22] T. Kosub, M. Kopte, R. Hühne, P. Appel, B. Shields, P. Maletinsky, R. Hübner, M. O. Liedke, J. Fassbender, O. G. Schmidt, and D. Makarov, "Purely antiferromagnetic magnetoelectric random access memory," Nat. Commun. **8**, 1–7 (2017).

[23] Y. Wang, X. Zhou, C. Song, Y. Yan, S. Zhou, G. Wang, C. Chen, F. Zeng, and F. Pan, "Electrical control of the exchange spring in antiferromagnetic metals," Adv. Mater. **27**, 3196–3201 (2015).

[24] P. X. Zhang, G. F. Yin, Y. Y. Wang, B. Cui, F. Pan, and C. Song, "Electrical control of antiferromagnetic metal up to 15 nm," Sci. China: Phys., Mech. Astron. **59**, 1–5 (2016).

[25] M. Goto, K. Nawaoka, S. Miwa, S. Hatanaka, N. Mizuochi, and Y. Suzuki, "Electric field modulation of tunneling anisotropic magnetoresistance in tunnel junctions with antiferromagnetic electrodes," Jpn. J. Appl. Phys. **55**, 080304 (2016).

[26] X. Chen, X. Zhou, R. Cheng, C. Song, J. Zhang, Y. Wu, Y. Ba, H. Li, Y. Sun, Y. You, Y. Zhao, and F. Pan, "Electric field control of Néel spin–orbit torque in an antiferromagnet," Nat. Mater. **18**, 931 (2019).

[27] L. Šmejkal, J. Železný, J. Sinova, and T. Jungwirth, "Electric control of dirac quasiparticles by spin-orbit torque in an antiferromagnet," Phys. Rev. Lett. **118**, 106402 (2017).

[28] P. Tang, Q. Zhou, G. Xu, and S. C. Zhang, "Dirac fermions in an antiferromagnetic semimetal," Nat. Phys. **12**, 1100–1104 (2016).

[29] U. Bauer, M. Przybylski, J. Kirschner, and G. S. D. Beach, "Magnetoelectric charge trap memory," Nano Lett. **12**, 1437–1442 (2012).

[30] U. Bauer, L. Yao, A. J. Tan, P. Agrawal, S. Emori, H. L. Tuller, S. van Dijken, and G. S. Beach, "Magneto-ionic control of interfacial magnetism," Nat. Mater. **14**, 174–181 (2015).

[31] D. Sztenkiel, M. Foltyn, G. Mazur, R. Adhikari, K. Kosiel, K. Gas, M. Zgirski, R. Kruszka, R. Jakiela, T. Li, A. Piotrowska, A. Bonanni, M. Sawicki, and T. Dietl, "Stretching magnetism with an electric field in a nitride semiconductor," Nat. Commun. **7**, 13232 (2016).

[32] J. Evertsson, F. Bertram, F. Zhang, L. Rullik, L. R. Merte, M. Shipilin, M. Soldemo, S. Ahmadi, N. Vinogradov, F. Carlà, J. Weissenrieder, M. Göthelid, J. Pan, A. Mikkelsen, J. O. Nilsson, and E. Lundgren, "The thickness of native oxides on aluminum alloys and single crystals," Appl. Surf. Sci. **349**, 826–832 (2015).

[33] P. Wadley, V. Novák, R. Campion, C. Rinaldi, X. Martí, H. Reichlová, J. Železný, J. Gazquez, M. Roldan, M. Varela, D. Khalyavin, S. Langridge, D. Kriegner, F. Máca, J. Mašek, R. Bertacco, V. Holý, A. Rushforth, K. Edmonds, B. Gallagher, C. Foxon, J. Wunderlich, and T. Jungwirth, "Tetragonal phase of epitaxial room-temperature antiferromagnet CuMnAs," Nat. Commun. **4**, 2322 (2013).

[34] P. Reichert, K. S. Kjær, T. Brandt Van Driel, J. Mars, J. W. Ochsmann, D. Pontoni, M. Deutsch, M. M. Nielsen, and M. Mezger, "Molecular scale structure and dynamics at an ionic liquid/electrode interface," Faraday Discuss. **206**, 141–157 (2018).

[35] M. Jitvisate and J. R. T. Seddon, "Direct measurement of the differential capacitance of solvent-free and dilute ionic liquids," J. Phys. Chem. Lett. **9**, 126–131 (2018).